



Contents lists available at ScienceDirect

Journal of Biomechanics

journal homepage: www.elsevier.com/locate/jbiomech
www.JBiomech.com

Microscale strain mapping demonstrates the importance of interface slope in the mechanics of cartilage repair

Rebecca M. Irwin^a, Tianyu Gao^b, Alexander J. Boys^b, Kyla Ortved^c, Itai Cohen^d, Lawrence J. Bonassar^{a,e,*}^a Nancy E. and Peter C. Meinig School of Biomedical Engineering, Cornell University, Ithaca, NY, United States^b Department of Materials Science and Engineering, Cornell University, Ithaca, NY, United States^c Comparative Orthopaedics Laboratory, Cornell University, Ithaca, NY, United States¹^d Department of Physics, Cornell University, Ithaca, NY, United States^e Sibley School of Mechanical and Aerospace Engineering, Cornell University, Ithaca, NY, United States

ARTICLE INFO

Article history:

Accepted 25 November 2020

Keywords:

Collagen
Raman spectroscopy
Glycosaminoglycans
Integration
Biomechanics
Composition
Elastography

ABSTRACT

Achieving lateral integration of articular cartilage repair tissue with surrounding native cartilage remains a clinical challenge. Histological and bulk mechanical studies have identified extracellular matrix components that correlate with superior failure strength, but it is unclear how local changes in geometry and composition at the repair interface affect tissue strains under physiologic loading. Here, we investigated the effects of local compositional and interface geometry on lateral cartilage repair integration by coupling microscale Raman spectroscopy and confocal elastography to measure tissue strains under compressive and shear loading. Histological integration assessments did not have significant relationships with interface strains under compressive loading ($p > 0.083$) and only the perimeter attachment score was trending towards statistical significance with the $|E_{xy}|$ strain tensor under shear loading ($p = 0.050$). Interface slope had a stronger correlation with local tissue strains under compressive and shear loading compared to compositional measures of GAG, collagen, or proteins (compressive loading $|E_{yy}|$ tensor: $R^2 = 0.400$ (interface slope), 0.005 (GAG), 0.024 (collagen), and 0.012 (protein); shear loading $|E_{xy}|$ tensor: $R^2 = 0.457$ (interface slope), 0.003 (GAG), 0.006 (collagen), and 0.000 (total protein)). These data support surgical publications detailing the need for vertical walls when debriding chondral defects. Current histological integration assessments and local compositional measures were insufficient for identifying the variation in interface strains under compressive and shear loading. Thus, our data points to the importance of controlling interface geometry at the time of surgery, which has implications for cartilage repair integration and long-term healing.

© 2020 Elsevier Ltd. All rights reserved.

1. Introduction

Despite the numerous treatment options for focal chondral defects (Hinckel et al., 2020; Orth et al., 2020), a remaining challenge is achieving lateral integration of the repair tissue with native tissue. Clinical assessments of lateral integration are performed via histological grading where lateral integration is defined as contact or apposition of the native and repair tissue. Lateral integration is required to prevent continued tissue degeneration as fissuring and vertical cracks in cartilage are hallmarks of osteoarthritis (Pritzker et al., 2006) and cracks negatively affect

cartilage mechanobiology and its load-bearing capacity (Komeili et al., 2020, 2019b). Histological assessments are the gold standard for determining the success of integrative repair where dramatic differences in both composition and interface geometry have been identified at the repair interface (Nixon et al., 2017; Roberts et al., 2003). While histological scoring systems identify gaps or fissuring at the interface (Mainil-Varlet et al., 2010; Ortved et al., 2015), this provides little information about the mechanical competence of the interface. As such, it is unclear the extent to which these histological assessments correlate with micromotion at the interface under loading.

The mechanical environment resulting from joint loading likely affects integrative repair as mechanical cues have been implicated in cartilage biological processes. Finite element analyses have identified displacement gradients at the repair interface under compressive loading (Ahsan and Sah, 1999; Wayne et al., 1991),

* Corresponding author at: Department of Biomedical Engineering, Cornell University, 237 Tower Road, Ithaca, NY 14853, United States.

E-mail address: lb244@cornell.edu (L.J. Bonassar).

¹ Current address: Department of Clinical Studies, New Bolton Center, University of Pennsylvania, Kennett Square, PA, United States.

which can lead to graft detachment. Local strain assessments in cartilage explants have provided detailed understanding of healthy and damaged tissue mechanical properties (Buckley et al., 2010; Griffin et al., 2015, 2014; Komeili et al., 2020, 2019a; Moo et al., 2018; Silverberg et al., 2014). Additionally, high strains in articular cartilage have been linked to negative biological consequences including cell death, apoptosis, and mitochondrial dysfunction (Bonnievie et al., 2018; Delco et al., 2018).

Prior investigations of cartilage repair integration have focused on elucidating which extracellular matrix (ECM) components contribute to integration strength. Collagen deposition and cellular activity at the interface has been linked to increased integration strength from in vitro investigations (DiMicco et al., 2002; Maher et al., 2010; Van De Breevaart Bravenboer et al., 2004). An in vivo equine cartilage repair study found that IGF-I did not improve tensile integration strength despite enhancing matrix composition and histological integration scores (Gratz et al., 2006). This study, and prior in vitro investigations, used bulk failure properties to measure mechanical integration, but these bulk failure measures are limited in spatial resolution and do not capture local tissue strains under physiologic loading.

To determine the role of ECM components in integration strength, previous studies utilized idealized geometries such as right cylinders, which do not capture the range of interface geometries observed in both human and animal in vivo studies (Nixon et al., 2017; Roberts et al., 2003). A canine in vivo study identified that beveled edges resulted in larger lesions after repair compared to vertical edges (Rudd et al., 1987). Debridement at the time of surgery results in a variety of angles at the interface of healthy tissue, however it is unclear what effect interface geometry has on interface mechanics and success of repair.

Recent investigations have coupled microscale mechanical testing with vibrational microspectroscopy to understand the relationship between composition and mechanical function in articular cartilage and meniscal entheses (Boys et al., 2019; DiDomenico et al., 2019; Silverberg et al., 2014). Additionally, microscale strain mapping has recently been utilized on cartilage repair interfaces in vitro (Irwin et al., 2019). Measuring local composition and strain fields of interfaces obtained from in vivo repair studies would elucidate how both ECM composition and interface geometry contribute to local mechanics. As such, the aim of this study was to spatially correlate local compositional data and interface slope to microscale tissue strains under compressive and shear loading from a clinically relevant in vivo equine cartilage repair model.

2. Methods

2.1. Cartilage repair model

Osteochondral samples from an 8 month in vivo equine cartilage repair model were obtained from 9 horses from a previous study (Ortved et al., 2015). Briefly, horses between 2 and 4 years old underwent surgery where full-thickness, 15 mm diameter osteochondral defects were created bilaterally in the lateral trochlear ridge of the femur and randomly treated with either: (1) fibrin only, (2) naïve chondrocytes in fibrin, or (3) AAV5-IGF-I transduced chondrocytes in fibrin (n = 3/group).

2.2. Histological scoring and bulk biochemical analyses

Histological scores and bulk biochemical data (GAG, DNA, and collagen type II) were obtained from a previously published study using these samples (see supplementary methods) (Ortved et al., 2015).

2.3. Tissue sample preparation

A block of articular cartilage roughly $3 \times 3 \times 1.4$ mm (WidthxLengthxDepth) was dissected across the repair interface to contain both native and repair tissue (n = 9, Fig. 1). Samples remained submerged in PBS for subsequent imaging and mechanical testing (further details found in supplemental methods).

As a control, native equine articular cartilage with no repair tissue was also sectioned from the talar osteochondral block at least 5 mm from the defect site (n = 2) and prepared as repair samples.

2.4. Interface slope quantification

A common goal in cartilage repair surgery is to create “vertical walls” when debriding the chondral defect. We quantified the extent to which this was true using confocal images. Interface slope is the extent of change in the orientation of the repair line between the native and repair tissue relative to the axis of the underlying bone. In this coordinate system, vertical walls would have a slope of 0, and an interface that was parallel to the bone would have an infinite slope. Interface slope was calculated using confocal images throughout the tissue depth at a resolution of 25 μ m by manually drawing a line at the repair interface using MATLAB software (Fig. 2A–D). Interface regions were identified from confocal images by a veterinary surgeon (K.O.). The curve was fit to a third-degree polynomial and the slope was calculated as the absolute value of the change in x over the change in y.

2.5. Raman spectroscopy

Raman imaging was performed to obtain compositional maps across the repair interface (Boys et al., 2019) (Renishaw InVia Confocal Raman microscope, n = 3; WITec Alpha300R Confocal Raman microscope, n = 8). Spectra were obtained using a 785 nm laser through a 20X water immersion objective lens that was submerged in PBS. A map approximately 2 mm by 1 mm was obtained for each sample across the repair interface at 25 μ m resolution. Laser power was set to 70 mW and spectra were collected with an 8 s integration time.

Compositional maps for glycosaminoglycans (GAG, 1017–1127 cm^{-1}), collagen (835–905 cm^{-1}), and proteins (1217.5–1293.5 cm^{-1}) were quantified using the peak area for the ranges listed (Fig. 2E,F). Peak areas were normalized to values in the deep zone of the native region of each sample (see supplemental methods). This normalization was performed in order to compare between samples as tissue composition of adult equine cartilage is comparable between individual animals (Brama et al., 1999; MacDonald et al., 2002).

2.6. Strain quantification

Microscale strains at the interface were obtained using a modified version of previously established protocols (Buckley et al., 2008; Irwin et al., 2019; Middendorf et al., 2017) involving fluorescent staining, mounting to a custom stage, and imaging with a confocal microscope (see supplemental methods). Samples were first axially compressed manually 5–12% by a glass plate with images taken to track tissue deformations (Fig. 1). Samples were allowed 30 min to fully relax, with final compressive strains of 7.3–11.0%. Oscillatory shear was then applied at an amplitude of 1% and a frequency of 1 Hz with images captured at 60 fps.

Confocal image sequences were analyzed using Ncorr, an open source 2D-digital image correlation software implemented in MATLAB, to obtain local tissue deformations under compression and shear (window radius: 100–165 μ m; grid spacing: 12.5–20.7 μ m) (Blaber et al., 2015). Local Green-Lagrange strains were calcu-

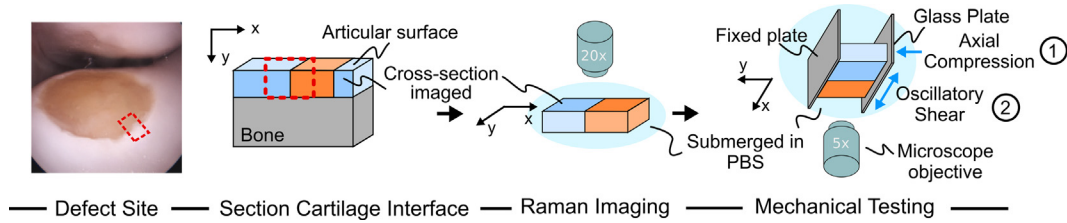


Fig. 1. Study design. Cartilage tissue was sectioned across the repair interface and imaged using Raman spectroscopy to obtain local tissue composition. Samples were first axially compressed (1) with images captured in real time to calculate tissue strains. After allowing the tissue to fully stress relax, an oscillatory shear was applied (2). Native tissue shown in blue, and repair tissue shown in orange. (For interpretation of the references to color in this figure legend, the reader is referred to the web version of this article.)

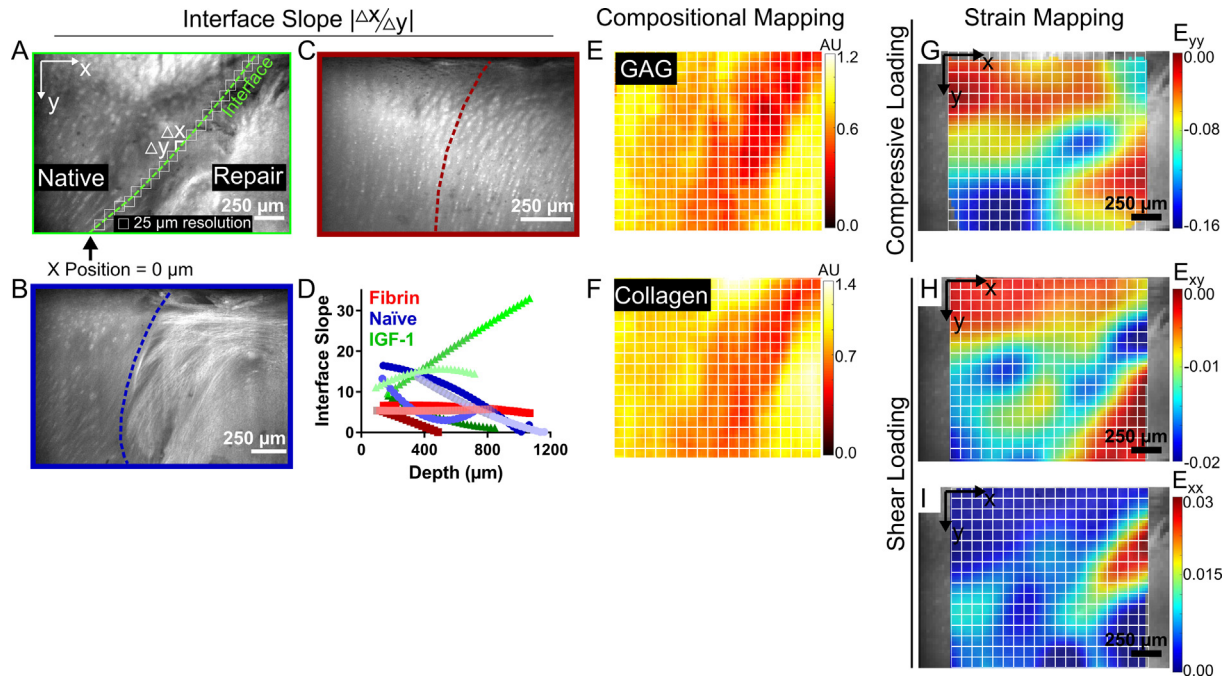


Fig. 2. Pixel-level registration of interface slope, composition, and strain. Interface slope was calculated through the tissue depth by fitting a polynomial to a manually drawn curve (A–D). Representative confocal images are shown for each treatment group with interface denoted by a dashed line (IGF-1: green; Naïve Chondrocyte: blue; Fibrin: red). Interface slopes as a function of tissue depth are shown for all samples (D). Composition maps of GAG and collagen were obtained from Raman spectroscopy (E,F). Microscale strains were spatially quantified under compressive and shear loading (G–I). Interface slope, strain maps, and compositional maps were all overlaid at matching resolutions of 25 μm . Scale bar = 250 μm .

lated by fitting a least squares plane on a subset of displacement data (window radius: 25.0–41.4 μm , Fig. 2G–I). Due to manual compression, there was variation in compressive strains (5–12%). To account for this, individual microscale strain observations were normalized to the bulk compressive strain applied for analyses of compressive loading.

2.7. Pixel-level spatial registration of interface slope, composition, and strain

To identify if local composition and interface slope correlated with strain behavior at the repair interface, data obtained from Raman mapping, slope calculation, and strain mapping were overlaid using a custom code in MATLAB. The white light image from Raman spectroscopy and the undeformed confocal image from compressive testing were uploaded into Inkscape for each sample. Features were manually matched optically in the two images (Middendorf et al., 2020). Raman data was recorded at a resolution of 25 μm , and the strain data was calculated at a resolution of 14.8–24.6 μm . In order to align the data sets, the strain data was binned

and averaged to align with the Raman data at a resolution of 25 μm .

2.8. Statistical analyses

Linear regression analyses were performed in PRISM software to compare bulk biochemical parameters by region to averaged interface strains. Kruskal-Wallis non-parametric tests were performed to compare histological scores to average interface strains using the R software package. The standard deviation of strains at the repair interface for control samples and all repair samples were compared to assess the variance in strain magnitudes using a one-way ANOVA and the data was log-transformed to achieve a normal distribution. A mixed linear model followed by an ANOVA was used to compare strain magnitudes at the repair interface between treatments where treatment was a fixed effect and horse was a random effect. Spatial Raman data and strain data in the native region was compared to the repair region for Naïve Chondrocyte and IGF-I treated groups using a mixed linear model followed by an ANOVA where region (native or repair) was a fixed effect and horse was a random effect. Data was log transformed.

Fibrin samples were not included in this analysis because data was taken from the perilesional region. A p-value < 0.05 was considered statistically significant.

3. Results

3.1. Average interface strains correlate with bulk GAG content but not histological integration scores

Bulk GAG, collagen, and DNA content were quantified in the perilesional, lesion, and remote sites of the defect and compared to average strains in a 250 μm wide region at the interface. Bulk GAG content in the perilesional region had a very strong correlation with average |E_{yy}| under compressive loading (R² = 0.834, p < 0.0001) and both average |E_{xy}| and average |E_{xx}| under shear loading (R² = 0.961, p < 0.0001 and R² = 0.830, p < 0.01, respectively). Additionally, DNA content in the remote region from the defect site had moderate correlations with average |E_{xy}| and average |E_{xx}| strains (p < 0.05, R² = 0.481 and R² = 0.473, respectively). There were no other significant relationships between strain tensors and bulk biochemical content for compressive or shear loading (Table 1).

Histological scores are the gold standard for assessing integrative repair, with the perimeter attachment score being used to

grade sections with no gaps (0), a gap at 1 side of the defect (1), or a gap at both sides of the defect (2) (Ortved et al., 2015). The perimeter attachment score did not have a significant relationship with |E_{yy}| under compressive loading (p = 0.083) and was trending towards significance with |E_{xy}| under shear loading (p = 0.050). No other histological score or strain tensor component for compressive or shear loading was significant with p-values greater than 0.1 (Table 2).

3.2. Compositional distributions show decreased GAG and collagen across repair interface

Similar to the strain distributions, the compositional distributions of GAG and collagen were constant across the x position for control samples (Fig. 3A-D). Collagen and protein data from Raman spectroscopy were highly correlated with each other (R² = 0.834, p < 0.0001, Supplemental Fig. 1), so only collagen data is displayed. The fibrin repair samples had decreased GAG content up to 1 mm away from the interface with normalized values ranging from 0.62 to 1.00 (Fig. 3E,F). In contrast, the collagen concentration remained constant ranging from normalized values of 0.79 to 1.14 up to 1 mm from the interface (Fig. 3G,H). In contrast to control samples, naïve chondrocyte and IGF-I repair treatments showed a decrease in GAG and collagen in the repair tissue compared to native tissue

Table 1

Bulk GAG and DNA content correlate with average strains at the repair interface. Multiple linear regression analysis of bulk biochemical parameters with average interface strains. R² values reported. Bold text denotes statistical significant (p < 0.05).

Bulk Biochemical Data	Compressive Loading				Shear Loading			
	E	E _{yy}	E _{xx}	E _{xy}	E	E _{yy}	E _{xx}	E _{xy}
Collagen Type II								
Lesion	0.060	0.054	0.040	0.000	0.094	0.051	0.017	0.260
Remote	0.055	0.037	0.030	0.045	0.004	0.103	0.003	0.157
DNA								
Lesion	0.352	0.531	0.070	0.301	0.527	0.123	0.092	0.501
Perilesion	0.075	0.221	0.001	0.034	0.189	0.087	0.260	0.131
Remote	0.084	0.267	0.001	0.222	0.439	0.039	0.473	0.481
GAG								
Lesion	0.120	0.025	0.166	0.021	0.078	0.023	0.011	0.095
Perilesion	0.434	0.834	0.005	0.023	0.904	0.133	0.830	0.961
Remote	0.010	0.003	0.010	0.141	0.129	0.242	0.116	0.066

Table 2

Histological scores evaluating cartilage repair do not capture local strains at repair interface. Kruskal-Wallis analysis of histology scores with components of the strain tensor under compressive and shear loading. P-values reported. The only parameter trending towards significance was the perimeter attachment score with |E_{xy}| under shear loading (outlined in table).

Histology Scores	Compressive Loading				Shear Loading			
	E	E _{yy}	E _{xx}	E _{xy}	E	E _{yy}	E _{xx}	E _{xy}
Defect Filling	0.424	0.271	0.446	0.416	0.482	0.294	0.462	0.620
Chond Predom	0.137	0.425	0.137	0.301	0.730	0.662	0.916	0.607
Periles Cloning	0.411	0.511	0.472	0.342	0.810	0.241	0.619	0.951
Subchond attach	0.485	0.446	0.485	0.337	0.299	0.325	0.458	0.519
Perimeter attach	0.537	0.083	0.870	0.842	0.067	0.294	0.275	0.050
Surface fib	0.949	0.981	0.759	0.243	0.554	0.189	0.610	0.337
Tidemark	0.327	0.462	0.142	0.221	0.389	0.902	0.902	0.221
Toluidine staining	0.915	0.434	0.450	0.619	0.545	0.662	0.288	0.867
Collagen type II	0.440	0.167	0.424	0.387	0.280	0.301	0.227	0.753
Total Score	0.434	0.434	0.434	0.434	0.434	0.434	0.434	0.434

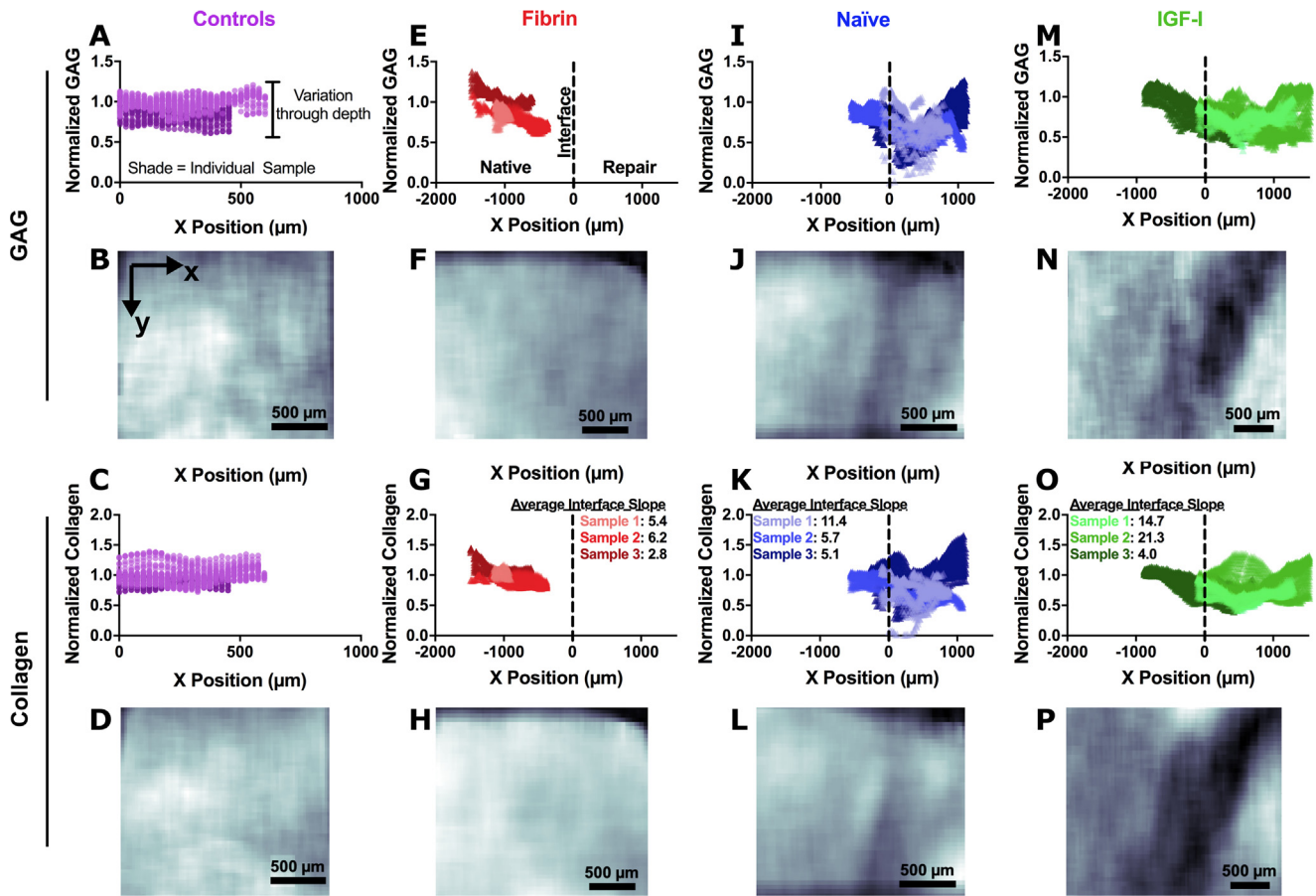


Fig. 3. Compositional distributions show decreased GAG and collagen across repair interface. Small variations in strains along the x position indicate consistency through the tissue depth. Dashed line at an x-position of 0 μm for repair samples denotes the location of the interface with native tissue on the left and repair tissue on the right. Each shade of color is an individual sample. The average interface slope values are provided for each sample in the corresponding treatment group panel. Control samples have constant GAG and collagen distribution across the repair interface (A-D). In the perilesional region, fibrin repair samples have decreased GAG starting up 1.5 mm from the repair interface while collagen remains constant (E-H). Naïve and IGF-I repair samples have decreased GAG and collagen across the interface and into repair tissue (I-P).

reaching minimum normalized values of 0.01 and 0.34 respectively (Fig. 3I-P, $p < 0.0001$).

3.3. Mapping of interface shows elevated strains in repair tissue

Control samples had constant strain values across the x position under compressive loading, ranging from 0.42 to 0.71 for $|E_{yy}|$ (Fig. 4A,F). In contrast, repaired samples had elevated strains up to 1.74 for $|E_{yy}|$ (Fig. 4B-D,G-I). Strain magnitudes in the repair region were elevated compared to the native region for naïve chondrocyte and IGF-I treatment groups for all strain tensor components ($p < 0.05$) except for the $|E_{yy}|$ tensor in the naïve chondrocyte treatment group ($p = 0.31$).

Similar to the compressive loading data, under shear loading tissue strains in the control samples did not vary with x position. Shear strains ($|E_{xy}|$) had a large range from 0.001 to 0.017 across the y position for control samples (Fig. 5A,B). This is expected for intact cartilage as shear strains are highest in the surface region of the tissue and then decrease with tissue depth along the y-axis (Supplemental Fig. 5). Repair tissue $|E_{xy}|$ strains varied with x position where the shear strain described a sliding motion between the repair and intact tissue (Fig. 5E,F,I,J,M,N). Peak lateral strains along the x-axis ($|E_{xx}|$) reached 0.004 in control samples, but ranged up to 0.026 for repair samples (Fig. 5G,H,K,L,O,P).

Tissue strains located in a 250 μm wide region at the repair interface described local movement under compressive and shear

loading. Repair samples had larger standard deviations in $|E_{yy}|$ compared to control samples under compressive loading (Fig. 4E, $p < 0.05$). There was large variance in strain magnitudes between horses in each treatment group, and as such no treatment was significantly different from controls (Fig. 4E, Fig. 5Q,R, $p < 0.30$).

3.4. Interface slope correlates with local strains better than compositional measures

For all three treatment groups, interface slope had a stronger correlation with local interface strains than compositional measures of GAG and collagen (Fig. 6). Under compressive loading, interface slope had a moderate correlation with the normalized axial compressive strains $|E_{yy}|$ in the 250 μm wide interface region ($R^2 = 0.400$, $p < 0.0001$, Fig. 6A). In contrast, both compositional measures of GAG and collagen had very weak correlations with $|E_{yy}|$ interface strains (GAG: $R^2 = 0.005$, $p = 0.0001$; collagen: $R^2 = 0.024$, $p < 0.0001$, Fig. 6B,C). Under shear loading, interface slope had a moderate correlation with $|E_{xy}|$ and a weak relationship with $|E_{xx}|$ under shear loading (Fig. 6D,G, $R^2 = 0.457$, $p < 0.0001$ and $R^2 = 0.323$, $p < 0.0001$ respectively). Measures of GAG and collagen had very weak correlations with $|E_{xy}|$ and $|E_{xx}|$ at the interface (Fig. 6E,F,H,I, GAG: $R^2 = 0.002$, $p < 0.01$ and $R^2 = 0.002$, $p = 0.01$; collagen: $R^2 = 0.006$, $p < 0.0001$ and $R^2 = 0.014$, $p < 0.0001$ respectively).

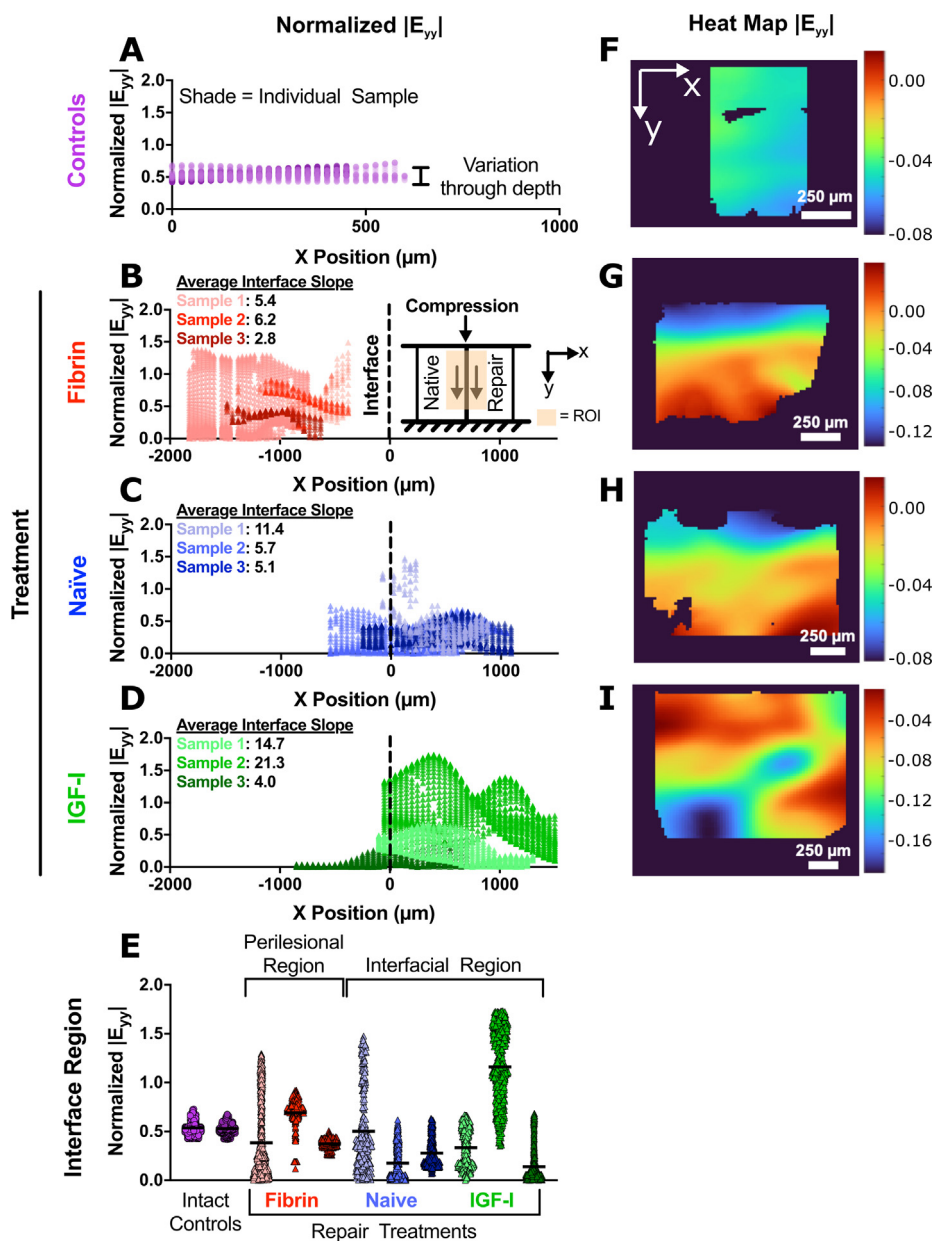


Fig. 4. Strain spatial distributions differ from controls for all treatment groups under compressive loading. Normalized tissue strains plotted across the x position of the tissue (A-D). Representative spatial maps of tissue strains for each treatment group are shown (F-I). Small variations in strains along the x position indicate consistency through the tissue depth. Dashed line at an x-position of 0 μm for repair samples denotes the location of the interface with native tissue on the left and repair tissue on the right. Each shade of color is an individual sample. The average interface slope values are provided for each sample in the corresponding treatment group panel. Range in strain magnitudes at a 250 μm wide region across the repair interface reveal high variability within samples (E).

4. Discussion

This study investigated the effects of local composition and interface geometry on lateral integration during articular cartilage repair in an eight month equine repair model. Microscale vibrational spectroscopy was coupled with confocal elastography to measure local collagen and GAG content and local strain fields during loading, respectively. Spatial variations in both composition and strain magnitudes were found across the x position of all repair samples regardless of treatment. Our results identified that interface slope was the predominant correlate with interface strains under compressive and shear loading, while GAG, collagen, and total protein content were only weakly correlated. Current histological integration assessments were insufficient for identifying the variation in interface strains under compressive loading. Col-

lectively, we identified interface slope as the primary driver of the mechanics at the repair interface under loading.

Quantifying local tissue strains provides a measure of motion at the interface of repair. Our experiments used physiologic levels of compressive strains (5–12%) and shear strain (1%) to characterize local strains similar to those experienced in vivo (Chan et al., 2016; Sanchez-Adams et al., 2014). Under the applied compressive strains, the Poisson's ratio was ~ 0.35 as expected for normal cartilage and was generally slightly lower for repaired tissues (presented as the lateral strain $|E_{xx}|$ as it was normalized to the axial strain $|E_{yy}|$, Supplemental Fig. 3). While physical detachment did not occur, repair treatments contained samples with elevated strains across the interface compared to intact controls. These differences in strain magnitudes and distributions have implications for integrative healing, as biological responses have been linked

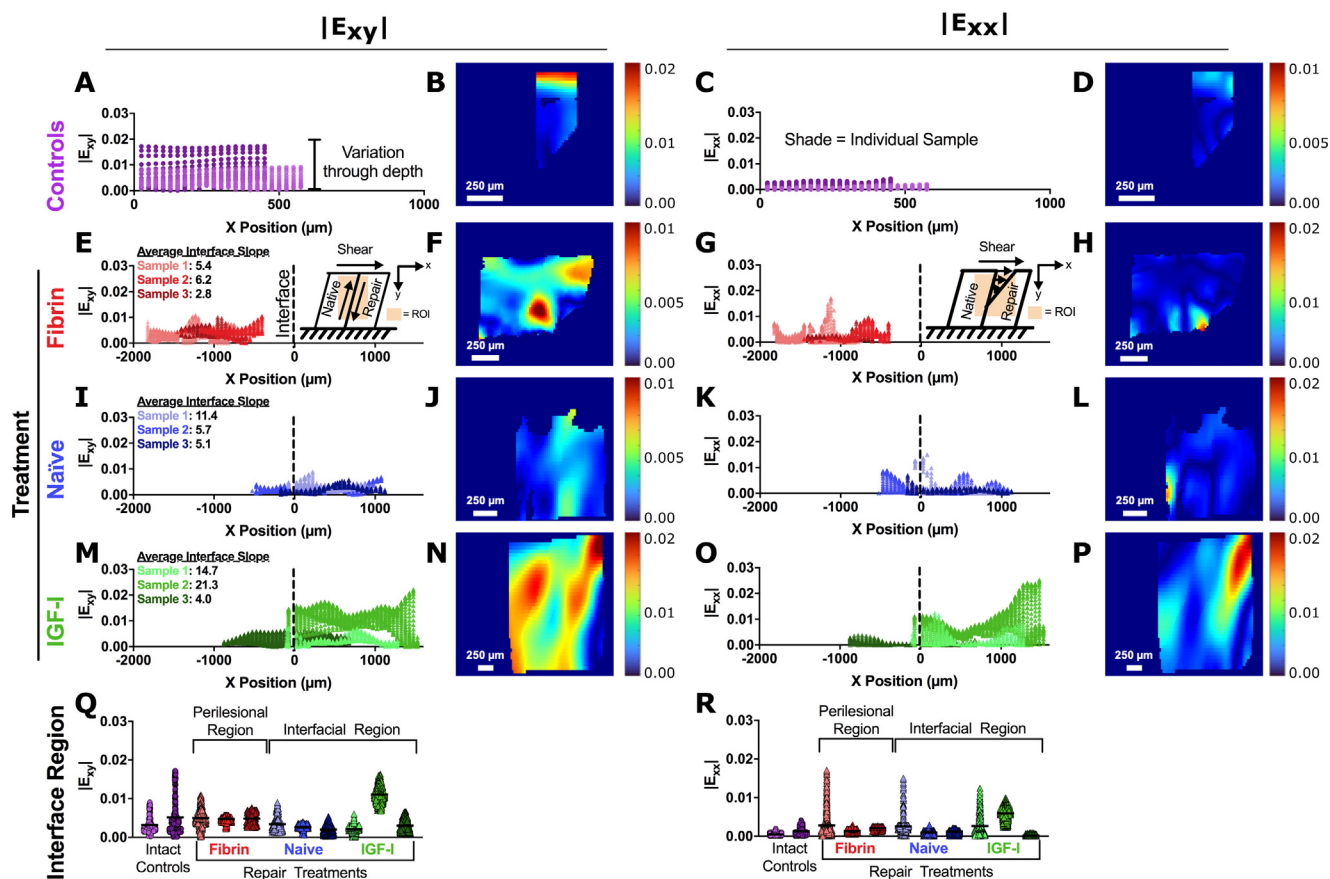


Fig. 5. Strain spatial distributions differ from controls for all treatment groups under shear loading. Normalized tissue strains plotted across the x position of the tissue (A,C,E, G,I,K,M,O). Small variations in strains along the x position indicate consistency through the tissue depth. Dashed line at an x-position of 0 μm for repair samples denotes the location of the interface with native tissue on the left and repair tissue on the right. Each shade of color is an individual sample. The average interface slope values are provided for each sample in the corresponding treatment group panel. Representative strain maps are shown for each treatment group (B,D,F,H,J,L,N,P). Range in strain magnitudes at a 250 μm wide region across the repair interface reveal high variability within samples (Q,R).

to impact and shear loading magnitudes (Bartell et al., 2015; Bonnevie et al., 2018). Therefore, altered biological responses at the interface are expected due to the varied strain magnitudes and spatial distributions.

Current integration assessments rely on histological scoring (Mainil-Varlet et al., 2010; Ortvad et al., 2015; Wang et al., 2016) and bulk biochemical measurements of composition at the repair interface (Fortier et al., 2002; Ortvad et al., 2015). Histological scoring systems assess only whether the interface is intact and thus give no insight into qualities of the interface that may affect mechanics. As such, our observation that histological assessments of integration were not correlated with local tissue strains was not surprising. Based on our results, we suggest that histological scoring systems could be altered to include a measurement of interface slope. Including such an assessment in a histological score would provide a relatively straightforward method for more accurately assessing lateral integration and could be characterized using standard staining.

Local GAG measurements from Raman spectroscopy had a very weak correlation with microscale tissue strains (length scale of 25 μm) while bulk GAG concentrations had a very strong correlation with average tissue strains (length scale 1 mm). GAG content is notoriously difficult to measure using Raman spectroscopy as the peak used for analysis has overlap with the B-type carbonate peak of collagen (Gamsjaeger et al., 2014). It is known that GAG content correlates with bulk mechanical properties in cartilage (Pfeiffer et al., 2008) and our results of average GAG and strain fol-

low this same trend. However, at the microscale, local variations in GAG do not appear to have a strong effect on the strain magnitudes. As such, bulk GAG assessments enable a prediction of average strain behavior at the repair interfaces whereas local GAG content is not predictive of local strains.

Previous in vitro and subcutaneous in vivo work has identified compositional features that correlate with improved integration. Collagen deposition (DiMicco et al., 2002), collagen cross-linking (Athens et al., 2013), and cellularity (Maher et al., 2010; Van De Breevaert Bravenboer et al., 2004) at the interface have all been implicated in integrative cartilage repair. These studies have identified useful models for elucidating the contributions of matrix deposition on integrative cartilage repair. A limitation of these models is the use of ideal geometries (i.e. vertical edges), which eliminate geometry as a variable and thus highlight correlations between bulk failure strength and compositional features. Our results show that the range of interface geometries present after cartilage repair surgery in vivo can outweigh the contributions of varying composition in determining local mechanics.

Many strategies have been employed to improve matrix deposition in articular cartilage defects including transfection of chondrocytes with growth factors such as IGF-I (Cucchiari et al., 2005; Kaul et al., 2006; Madry et al., 2010; Ortvad et al., 2015). As in previous studies using IGF-I transfection, there were notable differences between GAG levels across the interface between naïve chondrocyte- and IGF-I-treated samples. Despite significant enhancement in matrix deposition in IGF-I samples, there was no

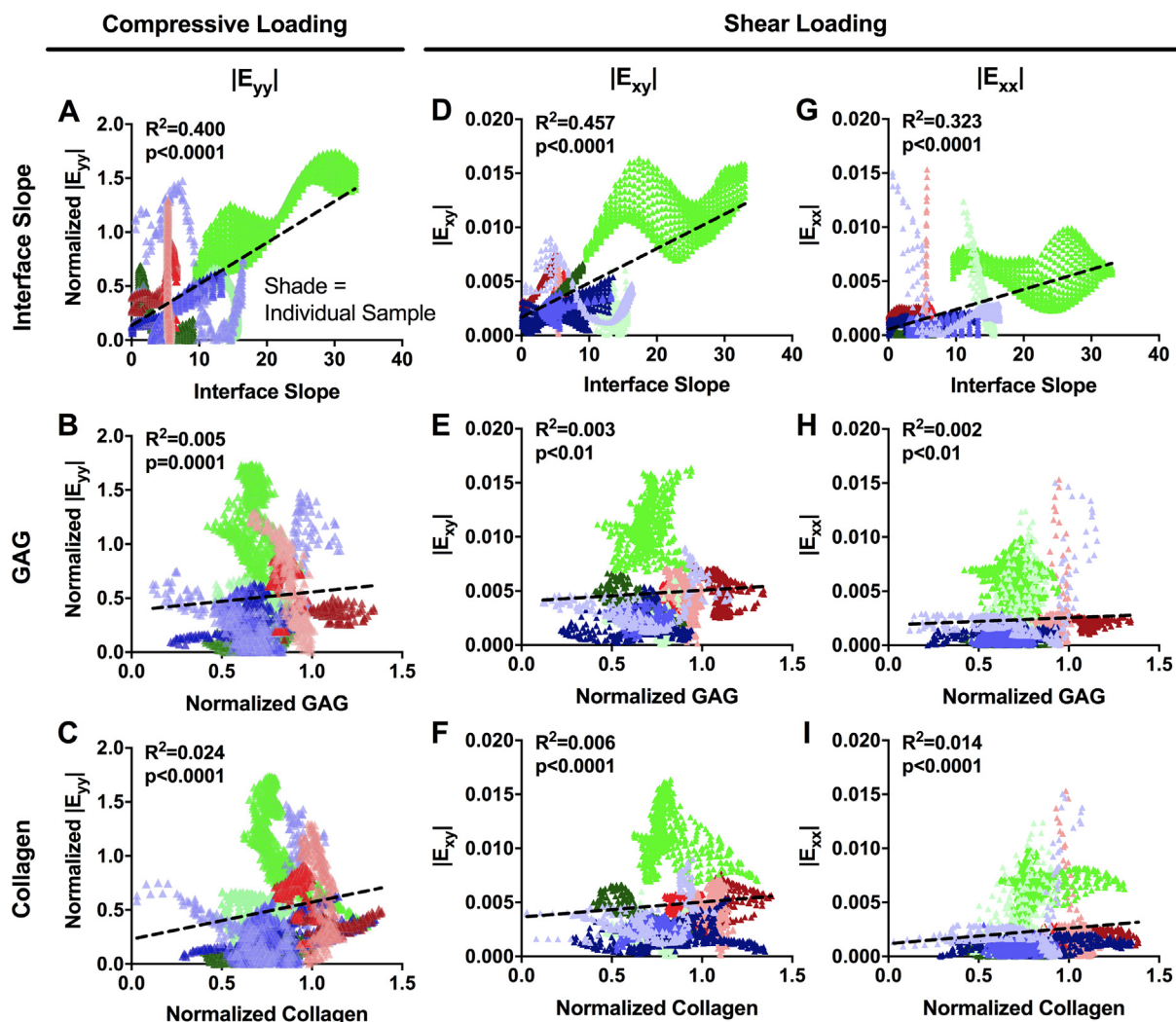


Fig. 6. Interface slope correlates with local strains better than compositional measures. Each data point is an individual observation within the 250 μm wide interface region. Color denotes treatment group (red: fibrin, blue: naïve chondrocytes, green: IGF-I). Shade denotes individual samples.

difference in repair integration between the three treatment groups evaluated in this study. This lack of difference arises from the variations in interface geometry present across the study. For example, the IGF-I sample #2 had elevated GAG deposition paired with a high slope resulting in high strain magnitudes at the interface. In contrast, the naïve chondrocyte sample #2 had decreased GAG content at the interface paired with a low slope corresponding to lower strains. Thus while enhancing matrix deposition is an important goal in cartilage repair, maintaining a vertical interface between the defect and native cartilage remains the predominant influence on interface mechanics. Notably, the primary importance of surgical factors in controlling interface mechanics is not true for other mechanical properties, such as bulk compressive, shear, and frictional properties, where treatment group is the dominant factor (Griffin et al., 2015). Collectively, these data suggest that different factors control bulk mechanics and tissue integration.

Previously published data on these samples found differences in the quality of the defect repair between the treatments, where the IGF-I samples had increased GAG content and bulk mechanical properties (Ortved et al., 2015). However, this enhancement of matrix deposition and bulk mechanics did not translate to any benefit in terms of tissue strains at the interface. An in vivo study of cartilage repair in equines evaluated injections of free IGF-I and found that while the IGF-I injection improved tissue repair quality and histological scoring (Fortier et al., 2002), there was no differ-

ence in tensile integration strength (Gratz et al., 2006). This was attributed to the fact that IGF-I stimulates GAG production and elevated GAGs are not likely to affect tensile cartilage properties. Here, we would expect increased GAG concentration to enhance tissue compressive properties, yet our findings show that the local increases in GAG content contributed minimally to local tissue strains as compared to interface slope.

Surgical publications detailing articular cartilage repair treatments stress the importance of creating vertical walls when debriding the defect (Alford and Cole, 2005; Bedi et al., 2010). A canine in vivo study also found that beveling the edges during debridement resulted in larger lesions and increased surface fibrillation (Rudd et al., 1987). The effect of defect angles of 100 or 80 were evaluated for intratissue strains during compression and stress relaxation in vitro, but both angles showed similar results (Gratz et al., 2009). Analogously, we found that similar deviations from a vertical wall yield comparable tissue strains near the interface. Collectively, our data and these previous studies strongly point to the necessity of creating vertical walls at debridement regardless of the cartilage repair treatment.

Prior finite element analyses have identified displacement gradients and increased fluid efflux caused by the differences in material properties across the interface (Ahsan and Sah, 1999; Wayne et al., 1991). Here, we also found strains in the repair region were significantly greater than in the native tissue. Our data are consis-

tent with these previous finite element studies and point to the need for continued simulations that examine the influence of interface geometry on the mechanics of cartilage repair.

There are several limitations to consider when interpreting these data. All strain data for the fibrin treated samples were obtained in the perilesional region, and therefore the fibrin treatment is confounded with the perilesional location for all interpretations and statistical measures. Comparing this fibrin repair data to controls, we identified changes in strain distributions and GAG composition up to 1 mm away from the interface that were not visible in the interface analyses. Tissue sections were obtained along one portion of the defect perimeter that grossly was identified as being intact. As such, alternative locations along the circumference of that defect for each horse could have altered geometries, compositions, and strains. However, our results identified correlations that were supported across all treatment groups, suggesting that these relationships would be true regardless of the site from which tissue was obtained. There were low samples sizes for each of the treatment groups ($n = 3/\text{group}$) and controls ($n = 2$). This limited our statistical power for comparing between horses and treatments. However, an advantage to our analytical method was the large data sets at the microscale level to compare tissue geometric and compositional features to mechanical behavior ($n = 402\text{--}2252$ observations per horse). Additionally, each repair sample included a native tissue region that served as an embedded control that behaved similarly to the virgin control cartilage and previous studies of equine cartilage (Griffin et al., 2016, 2015).

In this study, microscale spatial mapping was performed to identify if local tissue geometry and composition correlated with tissue strains under physiologic levels of compressive and shear loading. Local strains at the interface of cartilage repair were correlated with interface slope and bulk GAG content in the perilesional region. These data support surgical publications detailing the need for vertical walls when debriding chondral defects, and offer metrics that can be obtained using altered histological scoring and common biochemical measures to assess repair tissue integration. Thus, our data points to the importance of controlling interface geometry at the time of surgery, which has implications for cartilage repair integration and long-term healing.

Declaration of Competing Interest

The authors declare that they have no known competing financial interests or personal relationships that could have appeared to influence the work reported in this paper.

Acknowledgements

The authors would like to thank Françoise Vermeylen and Erika Mudrak from the Cornell Statistical Consulting Unit for their assistance with statistical analyses.

This work was supported in part by the NIH (R01AR071394-01), the NSF CMMI (1536463), and the Department of Education (GAANN Fellowship P200A150273 J). This work made use of the Cornell Center for Materials Research Shared Facilities which are supported through the NSF MRSEC program (DMR-1719875). A.J. B. would like to acknowledge a fellowship award (F31AR070009) from the National Institute of Arthritis and Musculoskeletal and Skin Diseases (NIAMS) of the National Institutes of Health (NIH).

Appendix A. Supplementary material

Supplementary data to this article can be found online at <https://doi.org/10.1016/j.jbiomech.2020.110159>.

References

- Ahsan, T., Sah, R.L., 1999. Biomechanics of integrative cartilage repair. *Osteoarthritis Cartil.* 7, 29–40. <https://doi.org/10.1053/joca.1998.0160>.
- Alford, J.W., Cole, B.J., 2005. Cartilage restoration, part 2: techniques, outcomes, and future directions. *Am. J. Sports Med.* 33, 443–460. <https://doi.org/10.1177/0363546505274578>.
- Athens, A.A., Makris, E.A., Hu, J.C., 2013. Induced collagen cross-links enhance cartilage integration. *PLoS ONE* 8. <https://doi.org/10.1371/journal.pone.0060719>.
- Bartell, L.R., Fortier, L.A., Bonassar, L.J., Cohen, I., 2015. Measuring microscale strain fields in articular cartilage during rapid impact reveals thresholds for chondrocyte death and a protective role for the superficial layer. *J. Biomech.* 48, 3440–3446. <https://doi.org/10.1016/j.jbiomech.2015.05.035>.
- Bedi, A., Feeley, B.T., Williams, R.J., 2010. Management of articular cartilage defects of the knee. *J. Bone Jt. Surg. - Ser. A.* <https://doi.org/10.2106/JBJS.100895>.
- Blaber, J., Adair, B., Antoniou, A., 2015. Ncorr: open-source 2D digital image correlation matlab software. *Exp. Mech.* 55, 1105–1122.
- Bonnevie, E.D., Delco, M.L., Bartell, L.R., Jasty, N., Cohen, I., Fortier, L.A., Bonassar, L.J., 2018. Microscale frictional strains determine chondrocyte fate in loaded cartilage. *J. Biomech.* 74, 72–78. <https://doi.org/10.1016/j.jbiomech.2018.04.020>.
- Boys, A.J., Kunitake, J.A.M.R., Henak, C.R., Cohen, I., Estroff, L.A., Bonassar, L.J., 2019. Understanding the stiff-to-compliant transition of the meniscal attachments by spatial correlation of composition, structure, and mechanics. *ACS Appl. Mater. Interfaces* 11, 26559–26570. <https://doi.org/10.1021/acsami.9b03595>.
- Brama, P.A., Tekoppele, J.M., Bank, R.A., van Weeren, P.R., Barneveld, A., 1999. Influence of site and age on biochemical characteristics of the collagen network of equine articular cartilage. *Am. J. Vet. Res.* 60, 341–345.
- Buckley, M.R., Bergou, A.J., Fouchard, J., Bonassar, L.J., Cohen, I., 2010. High-resolution spatial mapping of shear properties in cartilage. *J. Biomech.* 43, 796–800. <https://doi.org/10.1016/j.jbiomech.2009.10.012>.
- Buckley, M.R., Gleghorn, J.P., Bonassar, L.J., Cohen, I., 2008. Mapping the depth dependence of shear properties in articular cartilage. *J. Biomech.* 41, 2430–2437. <https://doi.org/10.1016/j.jbiomech.2008.05.021>.
- Chan, D.D., Cai, L., Butz, K.D., Trippel, S.B., Nauman, E.A., Neu, C.P., 2016. In vivo articular cartilage deformation: noninvasive quantification of intratissue strain during joint contact in the human knee. *Sci. Rep.* 6, 19220. <https://doi.org/10.1038/srep19220>.
- Cucchiari, M., Madry, H., Ma, C., Thurn, T., Zurakowski, D., Menger, M.D., Kohn, D., Trippel, S.B., Terwilliger, E.F., 2005. Improved tissue repair in articular cartilage defects in vivo by rAAV-mediated overexpression of human fibroblast growth factor 2. *Mol. Ther.* 12, 229–238. <https://doi.org/10.1016/j.ythm.2005.03.012>.
- Delco, M.L., Bonnevie, E.D., Bonassar, L.J., Fortier, L.A., 2018. Mitochondrial dysfunction is an acute response of articular chondrocytes to mechanical injury. *J. Orthop. Res.* 36, 739–750. <https://doi.org/10.1002/jor.23651>.
- DiDomenico, C.D., Kaghazchi, A., Bonassar, L.J., 2019. Measurement of local diffusion and composition in degraded articular cartilage reveals the unique role of surface structure in controlling macromolecular transport. *J. Biomech.* 82, 38–45. <https://doi.org/10.1016/j.jbiomech.2018.10.019>.
- DiMicco, M.A., Waters, S.N., Akeson, W.H., Sah, R.L., 2002. Integrative articular cartilage repair: dependence on developmental stage and collagen metabolism. *Osteoarthritis Cartilage* 10, 218–225. <https://doi.org/10.1053/joca.2001.0502>.
- Fortier, L.A., Mohammed, H.O., Lust, G., Nixon, A.J., 2002. Insulin-like growth factor-I enhances cell-based repair of articular cartilage. *J. Bone Jt. Surg. - Ser. B* 84, 276–288. <https://doi.org/10.1302/0301-620X.84B2.11167>.
- Gamsjaeger, S., Klaushofer, K., Paschalis, E.P., 2014. Raman analysis of proteoglycans simultaneously in bone and cartilage. *J. Raman Spectrosc.* 45, 794–800.
- Gratz, K.R., Wong, B.L., Bae, W.C., Sah, R.L., 2009. The effects of focal articular defects on cartilage contact mechanics. *J. Orthop. Res.* 27, 584–592. <https://doi.org/10.1002/jor.20762>.
- Gratz, K.R., Wong, V.W., Chen, A.C., Fortier, L.A., Nixon, A.J., Sah, R.L., 2006. Biomechanical assessment of tissue retrieved after in vivo cartilage defect repair: Tensile modulus of repair tissue and integration with host cartilage. *J. Biomech.* 39, 138–146. <https://doi.org/10.1016/j.jbiomech.2004.10.016>.
- Griffin, D.J., Bonnevie, E.D., Lachowsky, D.J., Hart, J.C.A., Sparks, H.D., Moran, N., Matthews, G., Nixon, A.J., Cohen, I., Bonassar, L.J., 2015. Mechanical characterization of matrix-induced autologous chondrocyte implantation (MACI®) grafts in an equine model at 53 weeks. *J. Biomech.* 48, 1944–1949. <https://doi.org/10.1016/j.jbiomech.2015.04.010>.
- Griffin, D.J., Orved, K.F., Nixon, A.J., Bonassar, L.J., 2016. Mechanical properties and structure-function relationships in articular cartilage repaired using IGF-I gene-enhanced chondrocytes. *J. Orthop. Res.* 34, 149–153. <https://doi.org/10.1002/jor.23038>.
- Griffin, D.J., Vicari, J., Buckley, M.R., Silverberg, J.L., Cohen, I., Bonassar, L.J., 2014. Effects of enzymatic treatments on the depth-dependent viscoelastic shear properties of articular cartilage. *J. Orthop. Res.* 32, 1652–1657. <https://doi.org/10.1002/jor.22713>.
- Hinckel, B.B., Pratte, E.L., Baumann, C.A., Gowd, A.K., Farr, J., Liu, J.N., Yanke, A.B., Chahla, J., Sherman, S.L., 2020. Patellofemoral cartilage restoration: a systematic review and meta-analysis of clinical outcomes. *Am. J. Sports Med.* <https://doi.org/10.1177/0363546519886853>.
- Irwin, R.M., Bonassar, L.J., Cohen, I., Matuska, A.M., Commins, J., Cole, B., Fortier, L.A., 2019. The clot thickens: Autologous and allogeneic fibrin sealants are

- mechanically equivalent in an ex vivo model of cartilage repair. *PLoS ONE* 14. <https://doi.org/10.1371/journal.pone.0224756>.
- Kaul, G., Cucchiari, M., Arntzen, D., Zurakowski, D., Menger, M.D., Kohn, D., Trippel, S.B., Madry, H., 2006. Local stimulation of articular cartilage repair by transplantation of encapsulated chondrocytes overexpressing human fibroblast growth factor 2 (FGF-2) in vivo. *J. Gene Med.* 8, 100–111. <https://doi.org/10.1002/jgm.819>.
- Komeili, A., Abusara, Z., Federico, S., Herzog, W., 2019a. Effect of strain rate on transient local strain variations in articular cartilage. *J. Mech. Behav. Biomed. Mater.* 95, 60–66. <https://doi.org/10.1016/j.jmbbm.2019.03.022>.
- Komeili, A., Chau, W., Herzog, W., 2019b. Effects of macro-cracks on the load bearing capacity of articular cartilage. *Biomech. Model. Mechanobiol.* 18, 1371–1381. <https://doi.org/10.1007/s10237-019-01149-x>.
- Komeili, A., Luqman, S., Federico, S., Herzog, W., 2020. Effect of cracks on the local deformations of articular cartilage. *J. Biomech.* 110. <https://doi.org/10.1016/j.jbiomech.2020.109970>.
- MacDonald, M.H., Tesch, A.M., Benton, H.P., Willits, N.H., 2002. Characterization of age- and location-associated variations in the composition of articular cartilage from the equine metacarpophalangeal joint. *J. Equine Vet. Sci.* 22, 25–32. [https://doi.org/10.1016/S0737-0806\(02\)70208-6](https://doi.org/10.1016/S0737-0806(02)70208-6).
- Madry, H., Orth, P., Kaul, G., Zurakowski, D., Menger, M.D., Kohn, D., Cucchiari, M., 2010. Acceleration of articular cartilage repair by combined gene transfer of human insulin-like growth factor i and fibroblast growth factor-2 in vivo. *Arch. Orthop. Trauma Surg.* 130, 1311–1322. <https://doi.org/10.1007/s00402-010-1130-3>.
- Maher, S.A., Mauck, R.L., Rackwitz, L., Tuan, R.S., 2010. A nanofibrous cell-seeded hydrogel promotes integration in a cartilage gap model. *J. Tissue Eng. Regen. Med.* 4, 25–29. <https://doi.org/10.1002/term.205>.
- Mainil-Varlet, P., Damme, B., Van, N., Nestic, D., Knutsen, G., Kandel, R., Md, J., Roberts, S., 2010. A new histology scoring system for the assessment of the quality of human cartilage repair: ICRS II. *Am. J. Sports Med.* 38, 880–890. <https://doi.org/10.1177/0363546509359068>.
- Middendorf, J.M., Dugopolski, C., Kennedy, S., Blahut, E., Cohen, I., Bonassar, L.J., 2020. Heterogeneous matrix deposition in human tissue engineered cartilage changes the local shear modulus and resistance to local construct buckling. *J. Biomech.* 109760. <https://doi.org/10.1016/j.jbiomech.2020.109760>.
- Middendorf, J.M., Shortkroff, S., Dugopolski, C., Kennedy, S., Siemiatkoski, J., Bartell, L.R., Cohen, I., Bonassar, L.J., 2017. In vitro culture increases mechanical stability of human tissue engineered cartilage constructs by prevention of microscale scaffold buckling. *J. Biomech.* 64, 77–84. <https://doi.org/10.1016/j.jbiomech.2017.09.007>.
- Moo, E.K., Sibole, S.C., Han, S.K., Herzog, W., 2018. Three-dimensional micro-scale strain mapping in living biological soft tissues. *Acta Biomater.* 70, 260–269. <https://doi.org/10.1016/j.actbio.2018.01.048>.
- Nixon, A.J., Sparks, H.D., Begum, L., McDonough, S., Scimeca, M.S., Moran, N., Matthews, G.L., 2017. Matrix-induced autologous chondrocyte implantation (MACI) using a cell-seeded collagen membrane improves cartilage healing in the equine model. *J. Bone Jt. Surg.* 99, 1987–1998. <https://doi.org/10.2106/JBJS.16.00603>.
- Orth, P., Gao, L., Madry, H., 2020. Microfracture for cartilage repair in the knee: a systematic review of the contemporary literature. *Knee Surgery, Sport. Traumatol. Arthrosc.* <https://doi.org/10.1007/s00167-019-05359-9>
- Ortved, K.F., Begum, L., Mohammed, H.O., Nixon, A.J., 2015. Implantation of rAAV5-IGF-I transduced autologous chondrocytes improves cartilage repair in full-thickness defects in the equine model. *Mol. Ther.* 23, 363–373. <https://doi.org/10.1038/MT.2014.198>.
- Pfeiffer, E., Vickers, S.M., Frank, E., Grodzinsky, A.J., Spector, M., 2008. The effects of glycosaminoglycan content on the compressive modulus of cartilage engineered in type II collagen scaffolds. *Osteoarthr. Cartil.* 16, 1237–1244. <https://doi.org/10.1016/j.joca.2008.02.014>.
- Pritzker, K.P.H., Gay, S., Jimenez, S.A., Ostergaard, K., Pelletier, J.-P., Revell, P.A., Salter, D., van den Berg, W.B., 2006. Osteoarthritis cartilage histopathology: grading and staging. *Osteoarthr. Cartil.* 14, 13–29. <https://doi.org/10.1016/j.joca.2005.07.014>.
- Roberts, S., McCall, I.W., Darby, A.J., Menage, J., Evans, H., Harrison, P.E., Richardson, J.B., 2003. Autologous chondrocyte implantation for cartilage repair: monitoring its success by magnetic resonance imaging and histology. *Arthritis Res. Ther.* 5, R60–R73. <https://doi.org/10.1186/AR613>.
- Rudd, R.G., Visco, D.M., Kincaid, S.A., Cantwell, H.D., 1987. The effects of beveling the margins of articular cartilage defects in immature dogs. *Vet. Surg.* 16, 378–383. <https://doi.org/10.1111/j.1532-950x.1987.tb00971.x>.
- Sanchez-Adams, J., Leddy, H.A., McNulty, A.L., O'Connor, C.J., Guilak, F., 2014. The mechanobiology of articular cartilage: bearing the burden of osteoarthritis. *Curr. Rheumatol. Rep.* 16, 451. <https://doi.org/10.1007/s11926-014-0451-6>.
- Silverberg, J.L., Barrett, A.R., Das, M., Petersen, P.B., Bonassar, L.J., Cohen, I., 2014. Structure-function relations and rigidity percolation in the shear properties of articular cartilage. *Biophysj* 107, 1721–1730. <https://doi.org/10.1016/j.bpj.2014.08.011>.
- Van De Breevaart Bravenboer, J., In Der Maur, C.D., Bos, P.K., Feenstra, L., An Verhaar, J., Weinans, H., Jvm Van Osch, G., 2004. Improved cartilage integration and interfacial strength after enzymatic treatment in a cartilage transplantation model. *Arthritis Res. Ther.* 6, 469–476. <https://doi.org/10.1186/ar1216>.
- Wang, C.-C., Yang, K.-C., Lin, K.-H., Liu, Y.-L., Yang, Y.-T., Kuo, T.-F., Chen, I.-H., 2016. Expandable scaffold improves integration of tissue-engineered cartilage: An *in vivo* study in a rabbit model. *Tissue Eng. Part A* 22, 873–884. <https://doi.org/10.1089/ten.tea.2015.0510>.
- Wayne, J.S., Woo, S.L.-Y., Kwan, M.K., 1991. Application of the u-p finite element method to the study of articular cartilage. *J. Biomech. Eng.* 113, 397–403. <https://doi.org/10.1115/1.2895418>.